

Tetratic order in the phase behavior of a hard-rectangle system

Aleksandar Donev,^{1,2} Joshua Burton,³ Frank H. Stillinger,⁴ and Salvatore Torquato^{1,2,4,*}¹*Program in Applied and Computational Mathematics, Princeton University, Princeton, New Jersey 08544, USA*²*PRISM, Princeton University, Princeton, New Jersey 08544, USA*³*Department of Physics, Princeton University, Princeton, New Jersey 08544, USA*⁴*Department of Chemistry, Princeton University, Princeton, New Jersey 08544, USA*

(Received 22 August 2005; revised manuscript received 5 December 2005; published 24 February 2006)

Previous Monte Carlo investigations by Wojciechowski *et al.* have found two unusual phases in two-dimensional systems of anisotropic hard particles: a tetratic phase of fourfold symmetry for hard squares [Comput. Methods Sci. Tech. **10**, 235 (2004)], and a nonperiodic degenerate solid phase for hard-disk dimers [Phys. Rev. Lett. **66**, 3168 (1991)]. In this work, we study a system of hard rectangles of aspect ratio two, i.e., hard-square dimers (or dominos), and demonstrate that it exhibits phases with both of these unusual properties. The liquid shows quasi-long-range tetratic order, with no nematic order. The solid phase we observe is a nonperiodic tetratic phase having the structure of a random tiling of the square lattice with dominos with the well-known degeneracy entropy $1.79k_B$ per particle. Our simulations do not conclusively establish the thermodynamic stability of this orientationally disordered solid; however, there are strong indications that this phase is glassy. Our observations are consistent with a two-stage phase transition scenario developed by Kosterlitz and co-workers with two continuous phase transitions, the first from isotropic to tetratic liquid, and the second from tetratic liquid to solid. We obtain similar results with both a classical Monte Carlo method using true rectangles and a novel molecular dynamics algorithm employing rectangles with rounded corners.

DOI: [10.1103/PhysRevB.73.054109](https://doi.org/10.1103/PhysRevB.73.054109)

PACS number(s): 03.65.Vf, 05.70.Fh, 03.75.Hh

I. INTRODUCTION

Hard-particle systems have provided a simple and rich model for investigating phase behavior and transport in atomic and molecular materials. It is long-known that a pure hard-core exclusion potential can lead to a variety of behaviors depending on the degree of anisotropy of the particles, including the occurrence of isotropic and nematic liquids, layered smectic, and ordered solid phases.¹ Through computer investigations of various particle shapes, other phases have been found, such as the biaxial² (recently synthesized in the laboratory³) and cubatic phases in three dimensions, in which the axes of symmetry of the individual particles align along two or three perpendicular axes (directors). One only need look at simple shapes in two dimensions to discover interesting phases. In recent work, Wojciechowski *et al.* studied hard squares and found the first example of a tetratic liquid phase at intermediate densities.⁴ In a tetratic liquid, there is (quasi)-long-range orientational ordering along two perpendicular axes, but only short-range translational ordering. The solid phase is the expected square lattice, with quasi-long-range periodic ordering. On the other hand, by studying hard-disk dimers (two disks fused at a point on their boundary), they have identified the first example of a nonperiodic solid phase at high densities.⁵ In this phase, the centroids of the particles are ordered on the sites of a triangular lattice. However, the orientations of the dimers are disordered, leading to a high degeneracy entropy of the nonperiodic solid and a lower free energy as compared to periodic solids. An experimental study of orientational ordering in nonequilibrium (quasi)-two-dimensional systems was recently performed using vibrated granular monolayers.⁶ It was found that the exact particle shape impacts the nature of the orientational ordering substantially, with tetratic ordering ap-

pearing for rectangles (monolayers of cylinders) even for high aspect ratios, and nematic ordering appearing for more rounded particles.

In this paper, we look at systems of rectangles of aspect ratio $\alpha=a/b=2$, where a and b are the semiaxes of the rectangle, i.e., hard-square dimers (or dominos). Since the aspect ratio is far from unity, it is not clear *a priori* whether nematic or tetratic orientational ordering (or both) will appear. Theoretical investigations of tetratic ordering, similar to Onsager's studies of nematic ordering, were performed by Zwanzig for a restricted-orientation model of a system of hard rods.⁷ Zwanzig found a phase transition into a nematic phase at sufficiently high densities for very elongated rods. The theory was, however, focused on three-dimensional systems of very elongated rods. Furthermore, restricted-orientation models have been shown to be misleading.⁸ Recent density functional theory calculations,⁹ extending previous work based on scaled-particle theory,¹⁰ have predicted that for $\alpha=2$ the tetratic phase is only metastable with respect to the ordered solid phase in which all particles are aligned. However, these calculations are only approximate and the authors point out that tetratic order is still possible in spatially ordered phases. An obvious candidate for forming a stable tetratic phase are dominos: two dominos paired along their long edges form a square, and these squares can then form a square lattice assuming one of two random orientations, thus forming a tetratic phase with degeneracy entropy of $\ln(\sqrt{2})$. In fact, one does not need to pair up the rectangles but rather simply tile a square lattice with dominos which randomly assume one of the two preferred perpendicular directions. The degeneracy entropy of this domino tiling has been calculated exactly to be $(2G/\pi)k_B \approx 0.58313k_B$,^{11,12} where $G = \sum_{n=0}^{\infty} (-1)^n (2n+1)^{-2} \approx 0.91597$ is Catalan's constant. At

high densities, free-volume theory¹ predicts that the configurational entropy (per particle) diverges as

$$S_{\text{FV}} \sim f \ln(1 - \phi/\phi_c) + S_{\text{conf}},$$

where f is the (effective) number of degrees of freedom per particle, ϕ_c is the volume fraction (density) at close packing, and S_{conf} is an additive constant due to collective exclusion-volume effects. Therefore, the densest solid is thermodynamically favored, but if several solids have the same density the additive factor matters. Therefore, for hard rectangles, for which the maximal density is $\phi_c=1$ and is achieved by a variety of packings, the degeneracy entropy can dominate S_{conf} and thus the nonperiodic random tiling can be thermodynamically favored. Indeed, our simulations of the hard-domino system produce high-density phases with structures very similar to that of a random covering of the square lattice with dimers. However, additional free-energy calculations and more sophisticated Monte Carlo simulations of the solid phase are necessary for definite answers.

The phase transitions in two-dimensional systems are of interest to the search for continuous Kosterlitz-Thouless-Halperin-Nelson-Young¹³⁻¹⁵ (KTHNY) transitions between the disordered liquid and the ordered solid phase. At present there is no agreement on the nature of the transition even for the hard-disk system. A previous study of the melting of a square-lattice crystal, stabilized by the addition of three-body interactions, found evidence of a (direct) first-order melting.¹⁶ Our observations for the domino system are relatively consistent with a KTHNY-like two-stage transition: a continuous phase transition from an isotropic to a tetratic liquid with long-range tetratic order around $\phi \approx 0.7$, and then another continuous transition from tetratic liquid to tetratic solid with quasi-long-range translational order at $\phi \approx 0.8$. However, we cannot rule out the possibility of a weak first-order phase transition between the two phases without more detailed simulations.

This paper is organized as follows. In Sec. II, we present the simulation techniques used to generate equilibrated systems at various densities. In Sec. III, we analyze the properties of the various states, focusing on the orientational and translational ordering in the high-density phases. We conclude with a summary of the results and suggestions for future work in Sec. IV.

II. SIMULATION TECHNIQUES

In this section, we provide additional details on the MC and MD algorithms we implemented. It is important to point out that it is essential to implement techniques for speeding up the near-neighbor search, in both MC and MD. For rectangles with a small aspect ratio, we employ the well-known technique of splitting the domain of simulation into cells (bins) larger than a particle diameter $D=2\sqrt{a^2+b^2}$, and consider as neighbors only particles whose centroids belong to neighboring cells. Additional special techniques more suitable for very aspherical particles or systems near jamming are described in Ref. 17.

A. Monte Carlo

We have implemented a standard MC algorithm in the NVT ensemble, with the additional provision of changing the density by growing or shrinking the particles in small increments. Each rectangle is described by the location of its centroid (x,y) and orientation θ . For increased computational speed the pair $(\sin \theta, \cos \theta)$ may be used to represent the orientation. In a trial MC step, a rectangle is chosen at random and its coordinates are changed slightly, either translationally $(\Delta x, \Delta y)$ or orientationally $(\Delta \theta)$. Every move has an equal chance of being translational or orientational. The rectangle's new position is then compared against nearby rectangles for overlap; if there is no overlap, the trial move is accepted. We call a sequence of N trials a cycle. The simulation evolves through stages, defined by a speed $n_{\text{cycles/stage}}$. At the end of a cycle, pressure data are collected by the virtual-scaling method of Eppenga and Frenkel.¹⁸ Namely, $p = PV/NkT = 1 + \phi\beta/2$, where β is the rate at which growing the particles causes overlaps. At the end of a stage, order parameters and other statistics are collected, and then the packing fraction ϕ is changed by a small value $\Delta\phi$; it may be increased, decreased, or not changed at all. If $\Delta\phi > 0$, then ϕ cannot necessarily change by $\Delta\phi$ every stage, because the increase could create overlaps. We scale down the increase by factors of 2 until a $\Delta\phi_{\text{eff}}$ is found that does not cause any overlaps when applied. Typical values for runs are $n_{\text{cycles/stage}} = 1000$ and $\Delta\phi = \pm 1 \times 10^{-5}$. Since there is a limit on how fast one can increase the density in such a Monte Carlo simulation, especially at very high densities, we use molecular dynamics to compress systems to close packing.

The overlap test is by far the largest computational bottleneck in the MC program. The overlap test for two rectangles is based on the following fact: Two rectangles R_1 and R_2 do not overlap if and only if a separating line l can be drawn such that all four corners of R_1 lie on one side of the line and all four corners of R_2 lie on the other side.¹⁹ The corners of both rectangles are allowed to coincide with l . Without loss of generality, we may assume l is drawn parallel to one of the rectangles' semiaxes and runs exactly along that rectangle's side. The problem of testing all possible lines l thus reduces to testing the eight lines that coincide with the edges of R_1 and R_2 . The test can be optimized somewhat further, as illustrated in Fig. 1. An axis \bar{a} of R_1 is chosen. The distance from the center of R_2 to \bar{a} is found. Then the distance d_0 of closest approach of R_2 to \bar{a} is found by subtracting a sine and a cosine; this distance corresponds to the corner of R_2 that is closest to \bar{a} . By comparing d_0 with the length b of the other semiaxis of R_1 , two possible lines l , corresponding to two opposite sides of R_1 , can be tested at once. If $d_0 < b$, there is an overlap. In this way, four different values of d_0 are calculated; one for each axis of each rectangle. If no comparison finds an overlap, there is no overlap.

B. Molecular dynamics

MC simulations are typically the most efficient when one is only interested in stable equilibrium properties. We have previously developed a molecular dynamics (MD) algorithm aimed at studying hard nonspherical particles and applied it

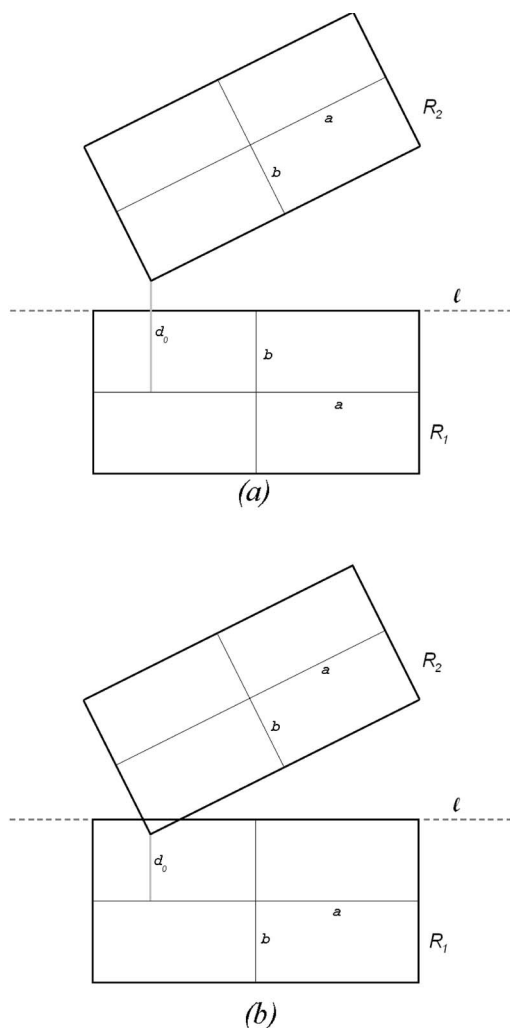


FIG. 1. Illustration of the optimized overlap test for two rectangles. The axes are \bar{a} and \bar{b} , with semiaxes a and b , and the length from \bar{a} to the closest corner of R_2 is d_0 . (Left) If $d_0 \geq b$, then the rectangles do not overlap. (Right) If $d_0 < b$, then the rectangles overlap.

to systems of hard ellipses and ellipsoids.¹⁷ We have since generalized the implementation to also handle “superellipses” and “superellipsoids,” which are generalized smooth convex shapes capable of approximating centrally symmetric shapes with sharp corners such as rectangles. A superellipse with semiaxes a and b is given by the equation

$$\left[\left| \frac{x}{a} \right|^{2\zeta} + \left| \frac{y}{b} \right|^{2\zeta} \right]^{1/\zeta} \leq 1,$$

where $\zeta \geq 1$ is an exponent. We add an exponent $1/\zeta$ above in order to properly normalize the convex function defining the particle shape, even though it is not strictly necessary. When $\zeta=1$ we get the simple ellipse, and when $\zeta \rightarrow \infty$ we obtain a rectangle with sides $2a$ and $2b$. The higher the exponent the sharper the corners become. The smoothing of the corners of the rectangle enables us to apply our collision-driven MD algorithm,¹⁷ with few changes from the case of ellipses. Details of this implementation will be given else-

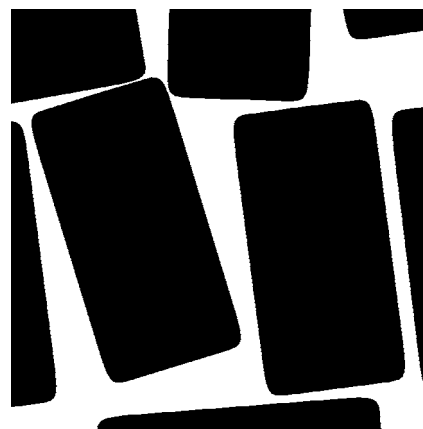


FIG. 2. An snapshot of a few superellipses (exponent $\zeta=7.5$) used in the MD simulations. It can be seen that the particle shape is very close to a rectangle.

where. The floating-point cost of the algorithm increases as the exponent increases, while the numerical stability decreases. We have used an exponent $\zeta=7.5$ for the studies presented here (for this exponent the ratio of the areas of the superellipse and the true rectangle is 0.9934). Figure 2 gives an illustration of the particle shape.

There are some advantages of the MD simulation over MC. The shapes of the particles can change arbitrarily fast in an easily controlled manner by simply adding a dynamic growth rate $\gamma=da/dt=\alpha db/dt$. If $\gamma>0$, i.e., the density is increasing, two colliding particles simply get an extra repulsive boost that ensures no overlaps are created. The velocities are periodically rescaled to $T=1$ to compensate for the induced heating or cooling due to the particle growth.¹⁷ In general, (common) MC methods do not work well near close packing, while MD methods, especially event-driven ones, can successfully be used to study the neighborhood of jamming points. Additionally, pressure measurement is more natural in the MD method, as the pressure can be directly obtained from time averages of the momentum exchange in binary collisions between particles. We have found this pressure measurement to be much more precise than using virtual particle scaling in MC simulations.

III. RESULTS

By using either the MC or the MD algorithm with small particle growth rate ($\Delta\phi$ or γ), we have traced the (quasi)-equilibrium phase behavior of systems of dominos over a range of densities. In this section, we present several techniques for measuring orientational and translational order for a given configuration of particles, as well as the results of such measurements for the generated states. We have tested our codes by first applying them to hard squares and comparing the results to those in Ref. 4, and we have observed good quantitative agreement throughout. Our MC pressure measurement systematically slightly underestimates the pressure compared to the NPT ensemble used in Ref. 4 and to our MD simulations. We present some of the results for the MC, and others for the MD simulations, marking any quan-

tative differences. The two techniques always produced qualitatively identical results.

Describing the statistical properties of the observed states would require specifying all of the n -particle correlation functions. The most important is the pair correlation function $g_2(r, \psi, \Delta\theta)$. Given a particle, $g_2(r, \psi, \Delta\theta)$ is the probability density of finding another particle whose centroid is a distance r away (from the centroid of the particle), at a displacement angle of ψ (relative to the first particle's coordinate axes), and with an orientation of $\Delta\theta$ (relative to the particle's orientation). The normalization of g_2 is such that it is identically unity for an ideal gas. We will use an equivalent representation where we fix a particle at the origin such that the longer rectangle axis is along the x axes, and represent pair correlations with $g_2(\Delta x, \Delta y, \Delta\theta)$, giving the probability density that there is another particle whose centroid is at position $(\Delta x, \Delta y)$ and whose major axis is at a relative angle of $\Delta\theta$. Since a three-dimensional function is rather difficult to calculate accurately and visualize, we can separate the translational and orientational components and average over some of the dimensions to reduce it to a one- or two-dimensional function.

The symmetry and nature of ordering in condensed phases is most easily accessed by using order parameters; specifically these would be scalar order metrics, which are typically averaged forms of local order parameters. Several types of order metrics are commonly applied in studies of two-dimensional hard-particle systems: orientational, bond-orientational, and translational order metrics, or combinations of orientational and bond-orientational order metrics.²⁰ We will present results for each of these types of ordering for the domino system. It would be useful to construct bond-orientational and translational order metrics that do not depend on splitting each domino into two squares in the future.

A. Equation of state

The pressure as a function of density can be most accurately measured in the MD simulations. There is no exact theory that can predict the entire equation of state (EOS) for a given many-particle system. However, there are two simple theories that produce remarkably good predictions for a variety of systems studied in the literature. For the isotropic fluid (gas) phase of a system of hard dominos, scaled-particle theory²¹ (SPT) predicts

$$p = \frac{1}{1 - \phi} + \frac{9}{2\pi} \frac{\phi}{(1 - \phi)^2}, \quad (1)$$

and modifications to account for possible orientational ordering are discussed in Refs. 9 and 10. For the solid phase, the free-volume (FV) theory predicts a divergence of the pressure near close packing of the form

$$p = \frac{3}{1 - \phi/\phi_c}, \quad (2)$$

and (liquid-state) density functional theory can be used to make quantitative predictions at intermediate densities.⁹ For superellipses with exponent $\zeta=7.5$ the maximal density is

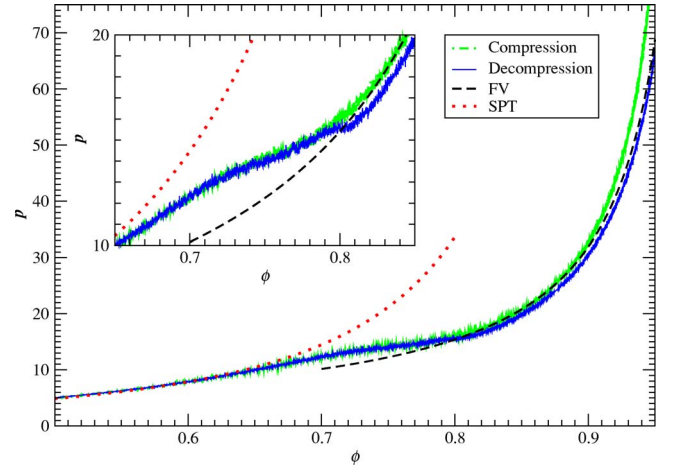


FIG. 3. (Color online) Reduced pressure $p = PV/NkT$ in a system of $N=5000$ superellipses with exponent $\zeta=7.5$ during MD runs with $\gamma = \pm 2.5 \times 10^{-5}$. The predictions of simple versions of SPT and FV theory are also shown for comparison. The agreement with FV predictions is not perfect; a numerical fit produces a coefficient 2.9 instead of 3 in the numerator of Eq. (2). Particularly noticeable are the change in slope around $\phi \approx 0.72$ and also the transition onto a solid branch well described by free-volume approximation around $\phi \approx 0.8$. Starting the decompression from an ordered tiling in which all rectangles are aligned produces identical pressure to within the accuracy available. Systems of $N=1250$ and $N=10\,000$ particles, as well as a wide range of particle growth rates, were investigated to ensure that there were no strong finite-size or hysteresis effects. In faster compressions of an isotropic liquid one gets smaller final densities due to the occurrence of defects such as vacancies or grain boundaries.

somewhat less than 1 and we take it to be equal to the ratio of the areas of the particle and a true rectangle $\phi_c \approx 0.9934$.

The numerical EOS from the NVT MD simulation are shown in Fig. 3 for both a slow compression starting from an isotropic liquid and a decompression starting from a perfect random domino tiling generated with the help of random spanning trees, as explained in Ref. 22. We note that the random domino tiling used was generated inside a square box (see Fig. 11) even though periodic boundary conditions were used in the actual simulation. We expect this to have a very small effect.²³ It is clearly seen from the figure that there is a transition from the liquid to the solid branch in the region $\phi \approx 0.7$ and $\phi \approx 0.8$, although no clear discontinuities or a hysteresis loop are seen (which would be indicative of a first-order phase transition). Compressing an isotropic liquid invariably freezes some defects and thus the jamming density is smaller (and the pressure is thus higher) than in the perfect crystal.

B. Orientational order

Orientational order can be measured via the orientational correlation function of order m

$$G_m(r) = \langle \cos(m\Delta\theta) \rangle_r, \quad (3)$$

where m is an integer and the average is taken over all pairs of particles that are at a distance between r and $r+dr$ apart

from each other. The one-dimensional function $G_m(r)$ can be thought of as giving normalized Fourier components of the distribution of relative orientations vs interparticle distance. When $m=2$, it measures the degree of nematic ordering (parallel alignment of the particles' major axes), and when $m=4$ it measures the degree of tetratic ordering (parallel alignment of the particles' axes). The infinite-distance value $\lim_{r \rightarrow \infty} G_m(r) = S_m$ gives a scalar measure of the tendency of the particles to align with a global coordinate system, S_2 is the usual nematic order parameter, and S_4 is the tetratic order parameter. They can be very easily calculated from an alternative definition

$$S_m = \max_{\theta_0} \langle \cos[m(\theta - \theta_0)] \rangle, \quad (4)$$

which can be converted into an eigenvalue problem (in any dimension) for the case $m=2$.²⁴ When $m=4$, we can rewrite it in the same form as $m=2$ by replacing θ with 2θ . The vector $\mathbf{n}_m = (\cos \theta_0, \sin \theta_0)$ determines a natural coordinate system for orientationally ordered phases. It is commonly called the director for nematic phases ($m=2$), and we will refer to it as a bidirector for tetratic phases ($m=4$).

In two-dimensional liquid-crystalline phases, it is expected that there can be no long-range orientational ordering, but rather only quasi-long-range orientational ordering.²⁵ Based on elasticity theory with a single renormalized Frank's constant $\tilde{K} = \pi K / (8k_B T)$, it is predicted²⁶ that there will be a power-law decay of the correlations at large distances, $G_m(r) \sim r^{-\eta}$, where

$$\eta = m^2 / 16K. \quad (5)$$

This would imply that S_m vanishes with increasing system size,

$$S_m \sim N^{-\eta/4}. \quad (6)$$

We note that this prediction is based on literature for the nematic phase. We are not aware of any theoretical work explicitly for a tetratic phase.

The KTHNY theories predict that the isotropic liquid first undergoes a defect-mediated second-order transition into an orientationally quasi-ordered but translationally disordered state when $\tilde{K}=1$ by disclination pair binding. At higher densities there is another second-order phase transition into a solid that has long-range orientational order and quasi-long-range translational order, mediated by dislocation pair binding. The validity of this theory is still contested even for hard disks,²⁷ and its applicability to systems where there is strong coupling between orientational and translational molecular degrees of freedom is questionable. Additionally, the basic theory needs to be modified to include three independent elastic moduli as opposed to only two in the case of six-fold rotational symmetry.

The observed change in S_4 as an isotropic liquid is slowly compressed is shown in Fig. 4 for both MD and MC runs. It is clearly seen that tetratic order appears in the system around $\phi \approx 0.7$ and increases sharply as the density is increased, approaching perfect order ($S_4=1$) at close packing. Throughout this run S_2 remains close to zero and thus no

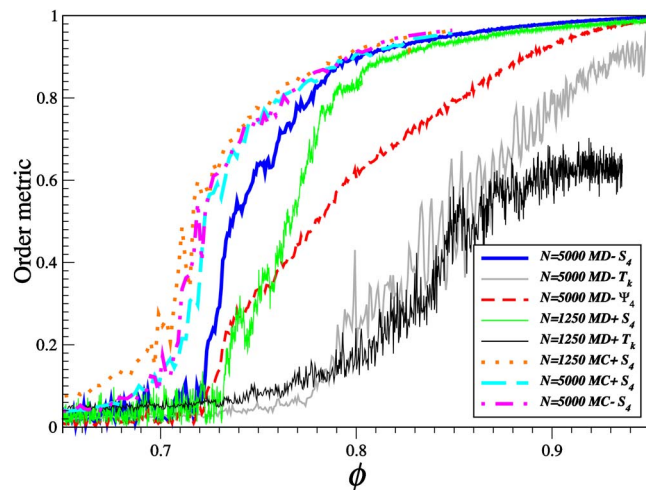


FIG. 4. (Color online) Values of the order metrics S_4 [see Eq. (4)], T_k [see Eq. (9)], and Ψ_4 [see Eq. (7)] for snapshot configurations along compression (marked with a plus sign in the legend) and decompression (marked with a minus sign) MC and MD runs. A transition in S_4 is visible around $\phi \approx 0.7$, and a transition in T_k is indicated around $\phi \approx 0.8$. The hysteresis between compression and decompression runs is stronger the larger the system size and the larger the expansion rate γ , especially in MD runs.

spontaneous nematic ordering is observed. It is important to note that superellipsoids are not perfect rectangles and have rounded sides. It is therefore not unexpected that they show less of a tendency toward tetratic (right-angle) ordering, and have the isotropic-tetratic (IT) transition at slightly higher densities. Additionally, the MD runs show more (correlated) variability due to the strong correlations between successive states (snapshots), and MD compressions lead to states with more pronounced defects. Therefore, we prefer to consider the MC results, other than at very high densities when we have to resort to MD studies. We have also performed runs decreasing the density of a random domino tiling, which has no nematic but has perfect tetratic order, and the resulting S_4 is also shown in the figure. Only a mild hysteresis is seen, especially for the MC runs, which would be indicative of a continuous IT transition, or at least a weakly discontinuous one. We note that we have never observed a phase boundary between a crystallized region and a disordered liquid, which would be indicative of a first-order phase transition.

Figure 5 shows $G_4(r)$ for a collection of states in the vicinity of the IT transition, thoroughly equilibrated using MC, on both a log-linear (lower densities) and a log-log (higher densities) scale. It is seen that there is a clear change in the long-range behavior of $G_4(r)$ as the density crosses above $\phi_c \approx 0.70$, from an exponential decay typical of an isotropic liquid, to a slower-than exponential decay at higher densities. The decay tails at higher densities are rather consistent with a power-law decay, and the fitted exponents η are shown in Fig. 6. It can be seen that η crosses the value $\eta_c=1$ predicted by KTHNY theory when $\phi \approx 0.71$, which is very consistent with the estimates of the location of the IT transition through the other methods above. It is not clear to us why the authors of Ref. 4 used the value of the exponent predicted by KTHNY theory for the bond-bond orientational

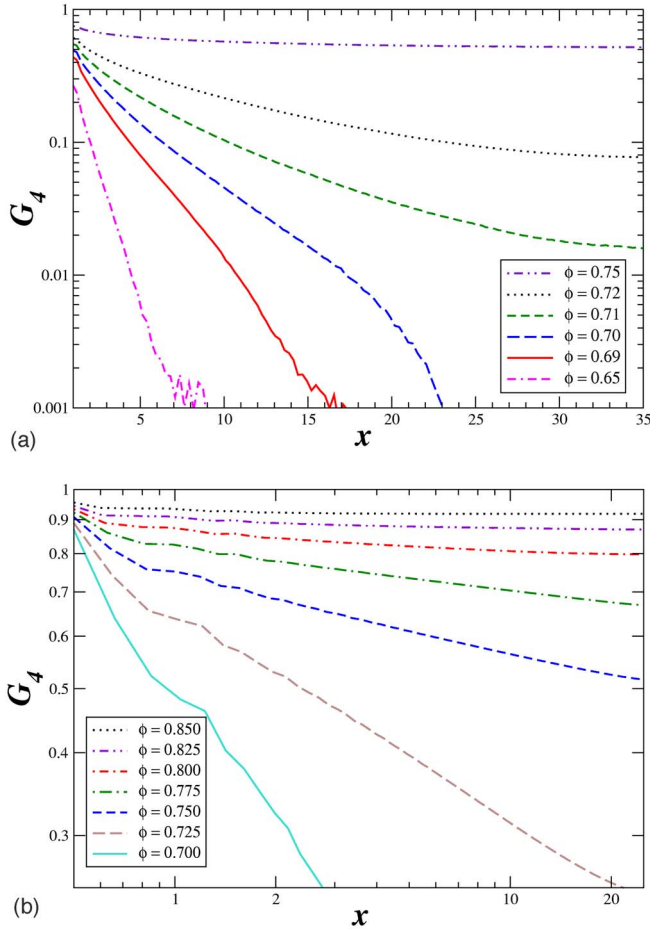


FIG. 5. (Color online) Top: Log-linear plot of $G_4(x)$ for thoroughly equilibrated samples of $N=10\,000$ particles, showing the decay of orientational ordering with distance $x=r/D$. The isotropic-tetratic transition occurs between $\phi=0.69$ and 0.70 , when the tail behavior of $G_4(r)$ changes from exponential (short-ranged) to slower than exponential. Bottom: Log-log plot of $G_4(x)$ for equilibrated systems of $N=5\,000$ particles, showing power-law decay indicative of quasi-long-range tetratic order. The fitted values of the power-law exponent are shown in Fig. 6.

order in the hard-disk system, $\eta_c=1/4$, instead of $\eta_c=1$. The somewhat higher values for S_4 for the system with $N=1250$ relative to the system with $N=5000$ particles are quantitatively well-explained by Eq.(6) using the values of η from Fig. 6. However, in order to unambiguously determine whether the decay in $G_4(r)$ is of a power-law form, larger systems should be studied and the scaling with system size determined carefully. Such studies are numerically very challenging and conflicting observations have been made even for the simplest case of hard disks. Unfortunately, for rectangles and superellipses, computational limitations presently prevent us from thoroughly equilibrating samples of more than 10 000 particles.

C. Bond-orientational order

It is geometrically intuitive that orientational ordering is related to translational ordering, especially for elongated par-

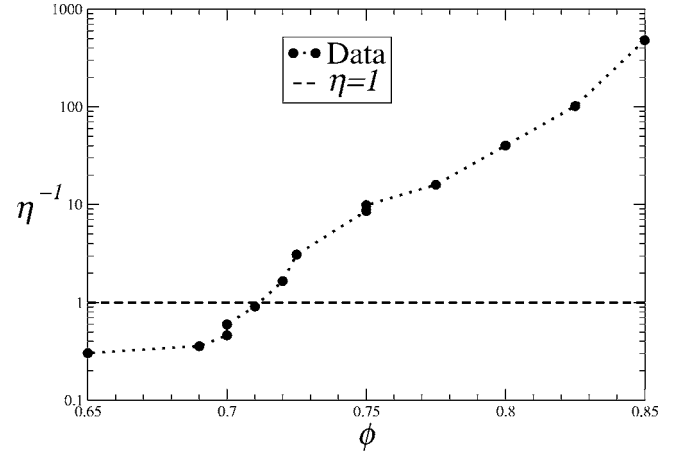


FIG. 6. Log-linear plot of $1/\eta$, where η is the exponent of decay of $G_4(r)$ found by fitting the $G_4(x)$ data in Fig. 5 to a power-law curve $G_4(x)=Cx^{-\eta}$.

ticles which need to coordinate orientational and translational degrees of freedom in order to avoid overlap at higher densities. From the observations above, we are motivated to look for translational order of the kind present in a random domino tiling. Looking at the centroids of the dominos themselves does not reveal a simple pattern. However, if we split each rectangle into two squares and look at the centroids of the $2N$ squares, translational order will be manifested through the appearance of an underlying square lattice.

From studies of other two-dimensional hard-particle systems, it has become clear that correlations between the orientations of the bonds connecting nearby particles can be (quasi) long ranged. We have measured the fourfold bond-orientational order in the system of $2N$ half-domino squares via the scalar order metric Ψ_4 defined by

$$\Psi_4 \exp(i\omega) = \frac{1}{2N} \sum_{i=1}^{2N} \frac{1}{N_{\text{neigh}}} \sum_{j=1}^{N_{\text{neigh}}} \exp(4i\theta_{ij}), \quad (7)$$

where θ_{ij} is the orientation of the line connecting the centroids of nearby squares, and the sum for each particle is over the 4 particles whose centroids are closest, i.e., $N_{\text{neigh}}=4$. Here ω is an angle giving the orientation of the global axes of fourfold alignment of the bonds. Other definitions of neighbors are possible. For example, Delaunay neighbors in the Voronoi tessellation of the point pattern formed by the centroids;²⁰ however, ambiguity is always present and the results are not very sensitive on the exact definition of neighbors so long as the average number of neighbors is close to 4. We find that for dominos, Ψ_4 qualitatively follows the behavior of S_4 very closely, as illustrated in Fig. 4, i.e., orientational ordering and bond-orientational ordering appear simultaneously, just as for the hard-square system.⁴

D. Translational order

Measuring (quasi)-long-range translational order is more difficult than measuring orientational or bond-orientational ordering. Translational order is typically manifested via the appearance of a long-ranged periodic pattern for the cen-

troids of the particles, in our case, the centroids of the half-dominos. Such periodicity is most easily quantified by the Fourier transform of the square (half-domino) centroids, i.e., the structure factor

$$S(\mathbf{k}) = \frac{1}{N} \left| \sum_{j=1}^N \exp(i\mathbf{k} \cdot \mathbf{r}_j) \right|^2. \quad (8)$$

In a translationally disordered state, $S(\mathbf{k})$ is of order 1 and decays to unity for large k . For long-ranged periodic systems, $S(\mathbf{k})$ shows sharp Bragg peaks at the reciprocal lattice vectors, while for quasi-long-range order the peaks have power-law wings. It is, however, difficult to exactly determine when true peaks replace the finite humps that exist due to short-range translational ordering in the liquid state.

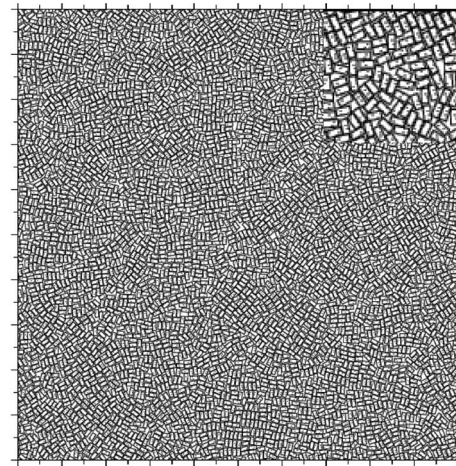
It would be convenient to have a scalar metric of translational order similar to S_4 for tetratic order. We use the averaged value of $S(\vec{k})$ over the first four Bragg peaks

$$T_k = \frac{1}{2N} \left[S\left(\frac{2\pi}{\tilde{a}} \mathbf{n}_{\parallel}\right) + S\left(\frac{2\pi}{\tilde{a}} \mathbf{n}_{\perp}\right) \right], \quad (9)$$

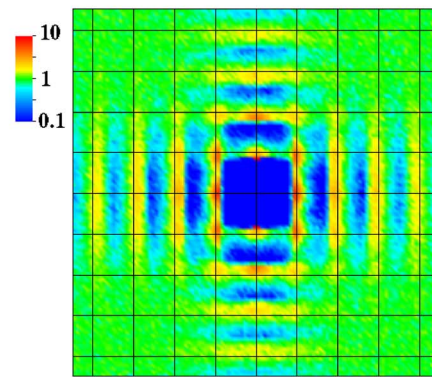
where $\tilde{a} = a/\sqrt{\phi}$ is the expected spacing of the underlying square lattice and \mathbf{n}_{\parallel} and \mathbf{n}_{\perp} are two perpendicular unit vectors determining the orientation of the square lattice. For a liquid $T_k \approx 0$, and in the tiling limit $T_k = 1$ (however, defects can disrupt periodicity and significantly reduce the value of T_k below unity). When decompressing a prepared tiling, we already know $\mathbf{n}_{\parallel} = (1, 0)$ and it is best to use this known value. However, when compressing a liquid, we have no way of knowing the final orientation of the lattice. We have tried using the bidirector $\mathbf{n}_{\parallel} = \mathbf{n}_4$, as determined during the measurement of S_4 . This method does not appear to work well because even small fluctuations in the director cause large fluctuations in T_k . Better results were obtained by using $\mathbf{n}_{\parallel} = (\cos \omega, \sin \omega)$ as determined from Eq. (7), as was done in Ref. 20; however, the large fluctuations remained. We therefore chose to do a brute-force search for the unit vector \mathbf{n}_{\parallel} that maximizes T_k , i.e., we rotate the presumed square lattice in small increments and find the optimal orientation.

A fundamental problem with T_k measured in this way is that it is smaller than unity away from the tiling limit even in a perfectly periodic domino system, since the two squares forming the domino are always closer than they would be if they were not glued together. In Fig. 4, we show the values of T_k along with S_4 . It is seen that for the decompression run, T_k starts at unity and decays continuously until it apparently goes to zero around $\phi \approx 0.8$. We are therefore led to believe that there is a second transition from tetratic liquid to tetratic solid at $\phi \approx 0.8$. However, the transition is not sharp and the value of T_k is already too small to confidently distinguish it from zero. It is therefore possible that translational ordering appears as soon as tetratic ordering does, around $\phi \approx 0.7$, as would be the case if a (mild) first-order phase transition existed around this density.

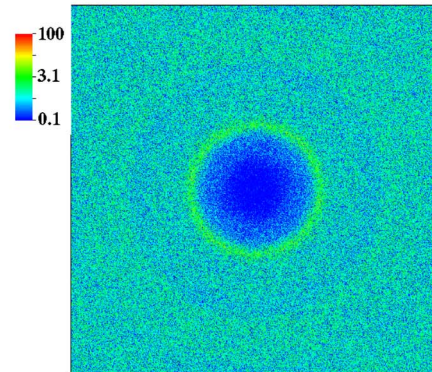
In addition to reciprocal space $S(\mathbf{k})$, one can also look at the center-to-center-distance distribution function $g_2(r)$ for the squares (half-dominos). However, quantitative analysis of $g_2(r)$ is made difficult because of oscillations due to ex-



(a)



(b)



(c)

FIG. 7. (Color online) A snapshot configuration of a system of $N=5000$ dominos at $\phi=0.7$ (top) with inset with threefold magnification showing local packing structure, along with $g_2(\Delta x, \Delta y)$ overlaid over the underlying square lattice (middle) and $S(\mathbf{k})$ (bottom), obtained after splitting each domino into two squares. It is clear that the system is isotropic from the rotational symmetry of $S(\mathbf{k})$. Only short-range order is visible in $g_2(\Delta x, \Delta y)$, confirming that this is an isotropic liquid.

clusion effects and also due to the coupling to orientation. Instead of presenting such a one-dimensional pair correlation function, we present $g_2(\Delta x, \Delta y)$, which is simply the orientationally averaged $g_2(\Delta x, \Delta y, \Delta \theta)$. In Figs. 7–9 we show a snapshot of a system of $N=5000$ dominos, along with the

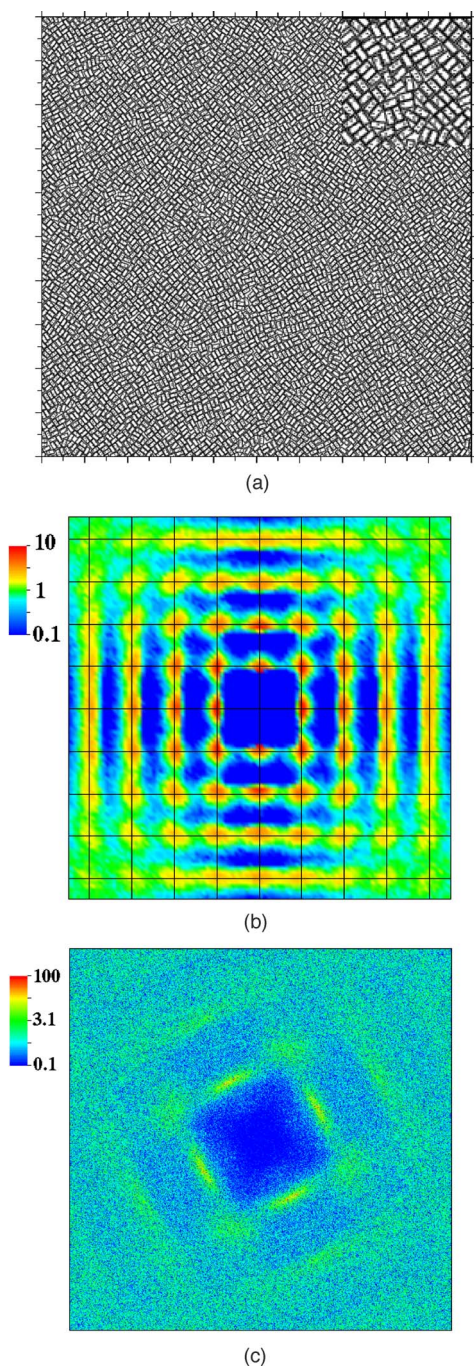


FIG. 8. (Color online) A system of $N=5000$ dominos as in Fig. 7 but at $\phi=0.750$, which shows a tetratic liquid phase. Fourfold broken symmetry is seen in $S(\mathbf{k})$, but without pronounced sharp peaks. The range of ordering in $g_2(r)$ has increased, but still appears of much shorter range than the size of the system, as seen clearly in the plot of the actual domino configuration. It is interesting that $g_2(\Delta x, \Delta y)$ is very anisotropic, being much stronger to the side of a square relative to its diagonals. No phase boundary characteristic of first-order transitions is visible.

corresponding $g_2(\Delta x, \Delta y)$ and $S(\mathbf{k})$, for three densities, corresponding to an isotropic liquid, a tetratic liquid [i.e., a state with (quasi)-long-range tetratic but only short-range translational order], and a tetratic solid [i.e., a state with (quasi)-

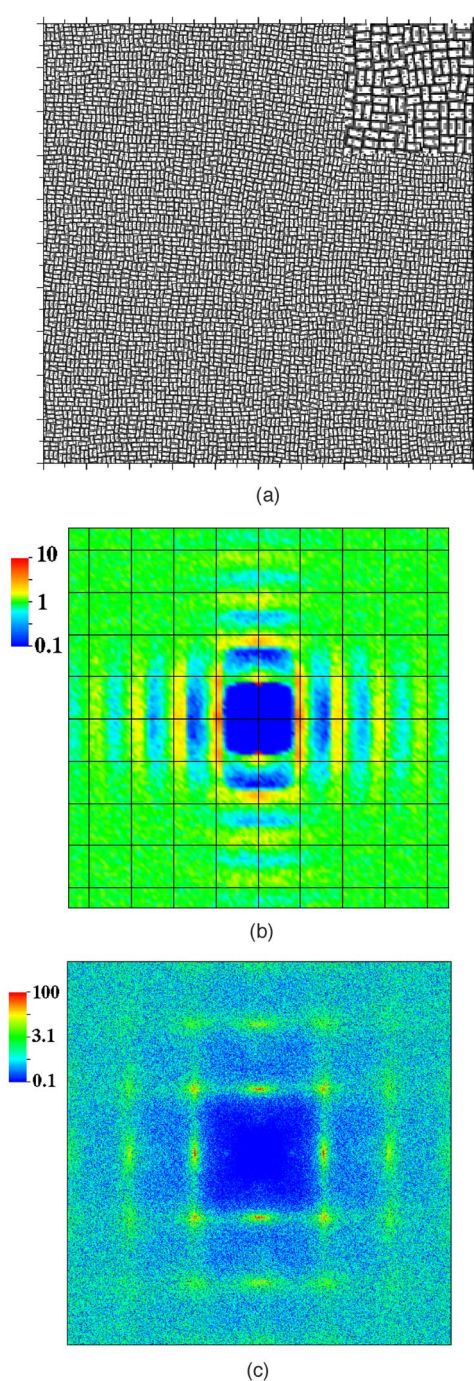


FIG. 9. (Color online) A system of $N=5000$ dominos as in Figs. 7 and 8 but at $\phi=0.825$. The structure factor shows sharp peaks (maximum value is above 10) on the sites of a (reciprocal) square lattice, and $g_2(r)$ shows longer-ranged translational ordering, indicating a solid phase. Visual inspection of the configuration confirms that the translational ordering spans the system size and shows some vacancies consisting of only a single square (half a particle).

long-range tetratic and translational order]. For the $g_2(\Delta x, \Delta y)$ plots, we have drawn the expected underlying square lattice at that density. Note that $g_2(\Delta x, \Delta y)$ always has two sharp peaks corresponding to the square glued to the one under consideration in the dimer (domino).

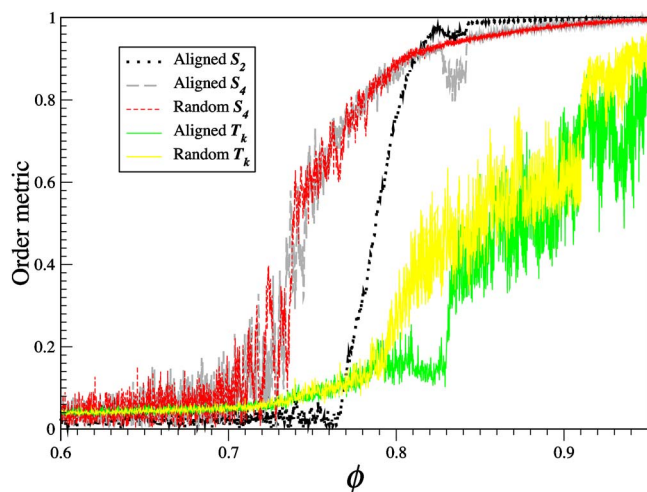


FIG. 10. (Color online) Nematic-, tetratic-, and translational-order metrics as a domino tiling in which all rectangles are aligned is slowly decompressed from close packing. The nematic crystal spontaneously realigned to a different orientation of the director from the starting one at around $\phi \approx 0.84$, causing some fluctuations and a drop in T_k which are likely just a finite-size (boundary) effect.

E. Solid phase

The investigations of ordering presented so far suggest that the domino system is very similar to the hard-square system⁴ when dominos are split into two squares. Essentially, around $\phi \approx 0.7$ the centroids of the squares form a disordered square lattice and their orientations align with the orientation of the square lattice, and the lattice itself orders over large distances at higher densities, leading to a tetratic solid. However, a fundamental question remains concerning the way in which the squares are joined to form the dominos in the thermodynamically stable solid phase. There are two likely possibilities: The tiling shows (translational) ordering itself, or the tiling is “random.” In the context of a discrete system such as domino tilings, the concept of a random tiling is mathematically well defined in terms of maximizing entropy.^{23,28} This random tiling has a positive degeneracy entropy $0.58313k_B$, unlike ordered tilings such as the nematic tiling (in which all dominos are aligned).

Our compressions of isotropic liquids have invariably led to apparently disordered domino tilings upon spontaneous “freezing,” albeit with some frozen defects. This suggests that the disordered tiling has lower free energy than ordered tilings. However, it is also possible that the disorder is simply dynamically trapped when the tetratic liquid freezes. In fact, starting a decompression run from an aligned nematic tiling shows that the tiling configuration is preserved until melting into a tetratic liquid occurs somewhat below $\phi \approx 0.8$. This is demonstrated in Fig. 10, where both S_4 and S_2 as well as T_k are shown along a decompression run starting with both a disordered and an ordered tiling. It is seen that S_2 drops sharply around $\phi \approx 0.8$ while S_4 remains positive until $\phi \approx 0.7$, clearly demonstrating the thermodynamic stability of the tetratic liquid phase in the intermediate density range. Subsequent compression of this liquid would lead to a disordered tiling without any trace of the initial nematic ordering.

It is intuitive to expect that the free-volume contribution to the free energy is minimized for ordered tilings at high densities. However, we also expect that solid phase is ergodic in the sense that transitions between alternative tiling configurations will occur in long runs of very large systems, so that in the thermodynamic limit the space of all tilings will be explored. This amounts to a positive contribution to the entropy of the disordered tiling due to its degeneracy, and it is this entropy that can thermodynamically stabilize the disordered tiling even in the close-packed limit. A closer analysis similar to that carried for hard-disk dimers in Refs. 5 and 29 is necessary. In particular, including collective Monte Carlo trial moves that transition between different tiling configurations, as well as relaxation of the dimensions of the unit cell (important for smaller solid systems), is important. Furthermore, only free-energy calculations can determine the free-volume entropies of various tiling patterns.

We conjecture that, just like the hard-disk dimer system, the hard-square dimer system has a thermodynamically stable nonperiodic solid phase. Even if this conjecture is false and the nematic phase is thermodynamically favored at sufficiently high densities, our simulations indicate that the dynamics is glassy; that is to say, the system gets trapped in disordered tilings even for very long runs, unlike the hard-disk system, where crystallization occurs easily. As in the hard dumbbell (fused hard-disk dimers) system, we expect that for aspect ratios close to, but not exactly, two, the nonperiodic solid will be replaced by a nematic (and possibly periodic) phase at the highest densities.^{29,30} This is because reaching the maximal density $\phi=1$ seems to require aligning the rectangles. It is interesting, however, that at least for rational, and certainly for integer aspect ratios such as $\alpha=3$, there is the possibility of disordered solid phases being stable even in the close-packed limit. On physical grounds we expect the phase diagram to vary smoothly with aspect ratio, rather than depending sensitively on the exact value of α , and the determination of the phase diagram around $\alpha=1$ and $\alpha=2$, even if only qualitatively, is an important challenge for future research.

Accepting for a moment the existence of a nonperiodic solid phase, it remains to verify that the compressed systems we obtain in our simulations are indeed similar to (maximal entropy) random tilings of the plane with dimers. This is hard to do rigorously, as it requires comparing all correlation functions between a random tiling and our compressed systems. Figure 11 shows a visual comparison of a random tiling of a large square, generated using random spanning trees by a program provided to us by the authors of Ref. 22, and a system of superellipses compressed to $\phi=0.95$ (close to the achievable maximum for our MD program for such high superellipse exponents). While the translational ordering in the compressed solid is clearly not perfect as it is for the true tiling, visual inspection suggests close similarity between the local tiling patterns of the two systems. Note that the primary type of defect that we observe are single-square vacancies, i.e., half-dominos missing from the true tiling of the plane. The number of vacancies observed during slow compressions is small and we do not expect it to affect thermodynamic properties significantly. In Fig. 12, we show $g_2(\Delta x, \Delta y)$ for the true tiling, along with the difference in g_2

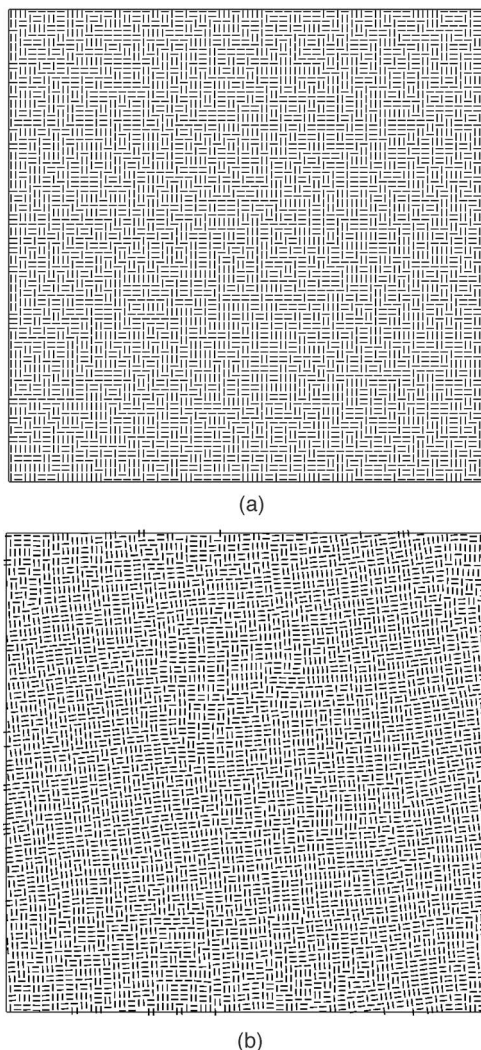


FIG. 11. A comparison between a true random tiling of a square with dominos (Ref. 22) (top), and the unit cell of a system of $N = 5000$ superellipses with exponent $\zeta = 7.5$ slowly compressed from isotropic liquid to $\phi = 0.95$ (bottom). The compressed system is not a perfect tiling due its lower density and frozen defects, as well as the rounding of the superellipses relative to true rectangles. Therefore at large scales the two systems look different. However a closer local examination reveals similar tiling patterns in the two systems, typical of “random” tilings.

between the true tiling and the compressed solid. Here we do not split the rectangles into two squares, i.e., the figure shows the probability density of observing a centroid of another rectangle at $(\Delta x, \Delta y)$ given a rectangle at the origin oriented with the long side along the x axis. It can be seen that there is a close match between the random tiling and the compressed solid, at least at the two-body correlation level.

IV. CONCLUSIONS AND FUTURE DIRECTIONS

The results presented in this paper highlight the unusual properties of the simple hard-rectangle system when the aspect ratio is $\alpha = 2$, hopefully stimulating further research into

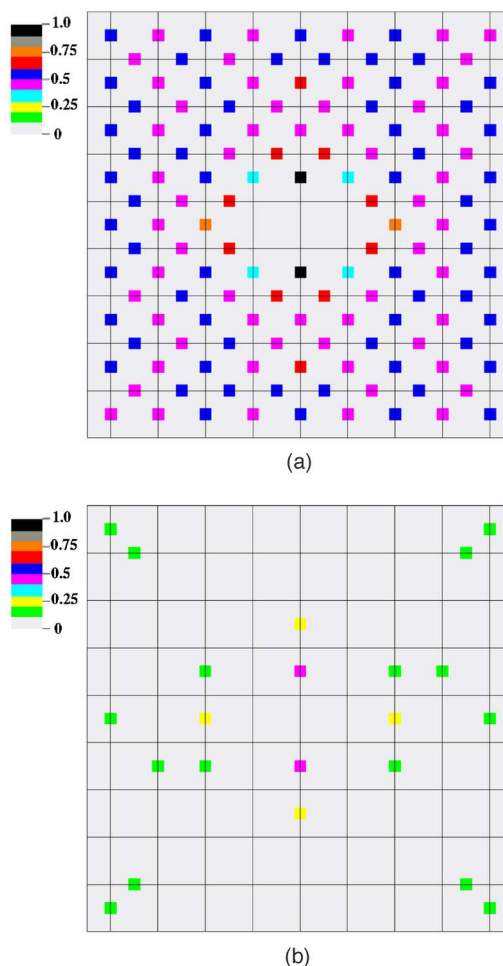


FIG. 12. (Color online) Top: Center-center pair correlation function $g_2(\Delta x, \Delta y)$ for the perfect random tiling in Fig. 11. This g_2 is a collection of Δ -functions whose heights can also be calculated exactly (Ref. 31) (the calculation is nontrivial and we have not performed it). We have normalized g_2 so that the highest peaks have a value of one. Bottom: The absolute value of the difference between $g_2(\Delta x, \Delta y)$ for the two systems shown in Fig. 11, shown on a coarse-enough scale so that the broadening of the peaks due to thermal motion is not visible. The color table used in this figure is discrete in order to highlight the symmetry and hide small fluctuations due to finite system size. The difference in g_2 is almost entirely within the smallest interval of the color table (less than 0.1, gray), with only some peaks showing differences up to 0.25.

the hard-rectangle system. For square dimers (dominos), in addition to the expected low-density isotropic liquid phase, a stable tetratic liquid phase is clearly observed, in which there is fourfold orientational ordering but no translational ordering. A tetratic solid phase closely connected to random domino tilings is observed and we conjecture that it is thermodynamically stabilized by its positive degeneracy entropy. The transitions between the phases are consistent with a KTHNY-like sequence of two continuous transitions. If this is indeed the case, then the hard dimer system provides an excellent model for the study of continuous transitions, with a rather large gap in density between the two presumed transitions $\Delta\phi \approx 0.1$, unlike the hard-disk system. Random

jammed packings of rectangles seem to be translationally ordered, similar to the behavior for disks³² but unlike spheres which can jam in disordered configurations.³³ However, unlike disks, the systems of rectangles show orientational disorder, once again illustrating the geometric richness of even the simplest hard-particle models.

Further investigations are needed for the domino system to conclusively determine its phase behavior. Improved MC with collective moves that explore multiple tilings, as well as allow for relaxation of the boundary conditions, should be implemented. Additionally, the free energies of the different phases should be computed so that the exact locations of the phase transitions could be identified. The final goal is to completely characterize the phase diagram of the hard rect-

angle system in the α - ϕ plane, as has been done, for example, for diskorectangles²⁶ and ellipses.³⁴ In addition to nematic and smectic phases, novel liquid crystal phases with tetratic order may be discovered.

ACKNOWLEDGMENTS

This work was supported in part by the National Science Foundation under Grant No. DMS-0312067. We thank Paul Chaikin for stimulating our interest in this problem and for numerous helpful discussions. We thank David Wilson for providing us with a program to generate random domino tilings (Ref. 22).

*Electronic address: torquato@electron.princeton.edu

¹J.-L. Barrat and J.-P. Hansen, *Basic Concepts for Simple and Complex Liquids* (Cambridge University Press, Cambridge, U.K., 2003).

²P. J. Camp and M. P. Allen, *J. Chem. Phys.* **106**, 6681 (1997).

³B. R. Acharya, A. Primak, and S. Kumar, *Phys. Rev. Lett.* **92**, 145506 (2004).

⁴K. W. Wojciechowski and D. Frenkel, *Comput. Methods Sci. Technol.* **10**, 235 (2004).

⁵K. W. Wojciechowski, D. Frenkel, and A. C. Brańka, *Phys. Rev. Lett.* **66**, 3168 (1991).

⁶V. Narayan, N. Menon, and S. Ramaswamy, cond-mat/0510082 (unpublished).

⁷R. Zwanzig, *J. Chem. Phys.* **39**, 1714 (1963).

⁸K. Shundyak and R. van Roij, *Phys. Rev. E* **69**, 041703 (2004).

⁹Y. Martínez-Ratón, E. Velasco, and L. Mederos, *J. Chem. Phys.* **122**, 014903 (2005).

¹⁰H. Schlacken, H.-J. Mogel, and P. Schiller, *Mol. Phys.* **93**, 777 (1998).

¹¹P. W. Kasteleyn, *Physica (Amsterdam)* **27**, 1209 (1961).

¹²H. N. V. Temperley and M. E. Fisher, *Philos. Mag.* **6**, 1061 (1961).

¹³J. M. Kosterlitz and D. J. Thouless, *J. Phys. C* **6**, 1181 (1973).

¹⁴D. R. Nelson and B. I. Halperin, *Phys. Rev. B* **19**, 2457 (1979).

¹⁵A. P. Young, *Phys. Rev. B* **19**, 1855 (1979).

¹⁶T. A. Weber and F. H. Stillinger, *Phys. Rev. E* **48**, 4351 (1993).

¹⁷A. Donev, S. Torquato, and F. H. Stillinger, *J. Comput. Phys.*

202, 737 (2005).

¹⁸R. Eppenga and D. Frenkel, *Mol. Phys.* **52**, 1303 (1984).

¹⁹S. Gottschalk, Ph.D. thesis, UNC Chapel Hill, Department of Computer Science, 2000.

²⁰T. Schilling, S. Pronk, B. Mulder, and D. Frenkel, *Phys. Rev. E* **71**, 036138 (2005).

²¹T. Boublík, *Mol. Phys.* **29**, 421 (1975).

²²R. W. Kenyon, J. G. Propp, and D. B. Wilson, *Electron. J. Comb.* **7**, R25 (2000).

²³H. Cohn, R. Kenyon, and J. Propp, *J. Am. Math. Soc.* **14**, 297 (2001).

²⁴R. J. Low, *Eur. J. Phys.* **23**, 111 (2002).

²⁵D. Frenkel and R. Eppenga, *Phys. Rev. A* **31**, 1776 (1985).

²⁶M. A. Bates and D. Frenkel, *J. Chem. Phys.* **112**, 10034 (2000).

²⁷H. Weber, D. Marx, and K. Binder, *Phys. Rev. B* **51**, 14636 (1995).

²⁸C. Richard, M. Höffe, J. Hermisson, and M. Baake, *J. Phys. A* **31**, 6385 (1998).

²⁹K. W. Wojciechowski, *Phys. Rev. B* **46**, 26 (1992).

³⁰K. W. Wojciechowski, *Phys. Lett. A* **122**, 377 (1987).

³¹R. Kenyon, *Ann. I.H.P. Probab. Stat.* **33**, 591 (1997).

³²A. Donev, S. Torquato, F. H. Stillinger, and R. Connelly, *J. Appl. Phys.* **95**, 989 (2004).

³³S. Torquato, T. M. Truskett, and P. G. Debenedetti, *Phys. Rev. Lett.* **84**, 2064 (2000).

³⁴J. A. Cuesta and D. Frenkel, *Phys. Rev. A* **42**, 2126 (1990).